DOI: 10.1016/j.matchemphys.2016.02.056



# IRON SULFIDE (TROILITE) INCLUSION EXTRACTED FROM SIKHOTE-ALIN IRON METEORITE: COMPOSITION, STRUCTURE AND MAGNETIC PROPERTIES

M.I. Oshtrakh[a,b,✉], Z. Klencsár[c], E.V. Petrova[a], V.I. Grokhovsky[a], A.V. Chukin[d], A.K. Shtoltz[e], A.A. Maksimova[a], I. Felner[f], E. Kuzmann[g], Z. Homonnay[g], V.A. Semionkin[a,b]

[a]*Department of Physical Techniques and Devices for Quality Control, Institute of Physics and Technology, Ural Federal University, Ekaterinburg, 620002, Russian Federation;*
[b]*Department of Experimental Physics, Institute of Physics and Technology, Ural Federal University, Ekaterinburg, 620002, Russian Federation;*
[c]*Institute of Materials and Environmental Chemistry, Research Centre for Natural Sciences, Hungarian Academy of Sciences, Magyar tudósok körútja 2, Budapest, 1117, Hungary;*
[d]*Department of Theoretical Physics and Applied Mathematics, Institute of Physics and Technology, Ural Federal University, Ekaterinburg, 620002, Russian Federation;*
[e]*Department of Electrophysics, Institute of Physics and Technology, Ural Federal University, Ekaterinburg, 620002, Russian Federation;*
[f]*Racah Institute of Physics, The Hebrew University, Jerusalem, Israel;*
[g]*Institute of Chemistry, Eötvös Loránd University, Budapest, Hungary*

DOI: 10.1016/j.matchemphys.2016.02.056

**Abstract**

Iron sulfide (troilite) inclusion extracted from Sikhote-Alin IIAB iron meteorite was examined for its composition, structure and magnetic properties by means of several complementary analytical techniques such as: powder X-ray diffractometry, scanning electron microscopy combined with energy-dispersive X-ray spectroscopy, magnetization measurements, ferromagnetic resonance spectroscopy and $^{57}$Fe Mössbauer spectroscopy with a high velocity resolution. The applied techniques consistently indicated the presence of daubréelite ($FeCr_2S_4$) as a minority phase beside troilite proper (FeS). As revealed by $^{57}$Fe Mössbauer spectroscopy, the Fe atoms in troilite were in different microenvironments associated with either the ideal FeS structure or that of a slightly iron deficient $Fe_{1-x}S$. Phase transitions of troilite were detected above room temperature by ferromagnetic resonance spectroscopy. A novel analysis of 295 and 90 K $^{57}$Fe Mössbauer spectra was carried out and the hyperfine parameters associated with the ideal structure of troilite were determined by considering the orientation of the hyperfine magnetic field in the eigensystem of the electric field gradient at the $^{57}$Fe nucleus.

***Keywords:*** Inorganic compounds; X-ray diffraction; Electron paramagnetic resonance; Mössbauer spectroscopy

---

✉Author for correspondence, E-Mail: oshtrakh@gmail.com

DOI: 10.1016/j.matchemphys.2016.02.056

## 1. Introduction

Iron sulfide FeS (troilite) is very rare material found at the Earth [1] while often found in various extraterrestrial objects, from meteorites to cosmic dust particles, in particular, in iron meteorites [2–5]. Iron meteorites based on Fe–Ni–Co alloy contain elements such as: P, S and C. Their presence leads to the formation of precipitates of iron-nickel phosphides $(Fe,Ni)_3P$ in the form of schreibersite and rhabdite and/or iron sulfide and iron-nickel carbides. These elements play an important role in the cooling rate of the metal melt (see [6]). Therefore, the study of the former precipitates in various iron meteorites is of interest for the analysis of the origin, composition and formation processes of iron meteorites as well as their thermal and impact history. As Goldstein et al. [6] mentioned, sulfur is virtually insoluble in solid metal and thus is found only in the form of inhomogeneously distributed troilite inclusions that likely represent melt trapped during the crystallization process. Troilite is a mineral which is the end-member of the pyrrhotite group with stoichiometric FeS or non-stoichiometric ($Fe_{1-x}S$) content. At ambient temperatures the crystal structure of troilite is hexagonal ( $P\bar{6}2c$ ) – as demonstrated by investigations of troilite from various meteorites (iron, chondrites) and synthetic analogues (see, for instance, [7–11] and references therein). On heating, troilite transforms into the orthorhombic MnP-type structure (*Pnma*) at around $T_\alpha \approx 413$ K, and successively to the hexagonal NiAs-type structure ($P6_3/mmc$) at ~483 K (see [8, 10] and references therein).

In addition to the crystal structure, information on the atomic level structure of iron bearing mineral phases in meteorites can be gained using Mössbauer spectroscopy (see, e.g., [8–10]). However, the accurate decomposition of the $^{57}$Fe Mössbauer spectra of bulk meteoritic samples is often made difficult by the presence of several iron bearing mineral phases and the overlap of their respective Mössbauer spectral components, e.g., in the case of ordinary chondrites [12–21]. Non-stoichiometry in troilite can lead to a multitude of different iron microenvironments, which results in further difficulties concerning the exact analysis of Mössbauer spectra. Even in the case of

DOI: 10.1016/j.matchemphys.2016.02.056

stoichiometric troilite, special attention has to be paid to the orientation of the hyperfine magnetic field with respect to the electric field gradient during spectral analysis. Namely, if we do not take into account the possible non-collinearity of the hyperfine magnetic field and the principal axis of electric field gradient, it is not possible to fit the Mössbauer spectrum of troilite correctly [7–9, 13, 16]. Accurate determination of the Mössbauer parameters of troilite in meteorite samples is important because they are supposed to reflect the conditions of crystallization of the parent body of the corresponding meteorites [16]. In the present work we also deal with the above mentioned problems of the troilite spectrum fit in a novel way for more reliable analysis of iron sulfide.

Sikhote-Alin IIAB iron meteorite contains some minor iron bearing inclusions in kamacite matrix such as iron-nickel phosphides $(Fe,Ni)_3P$ in the forms of schreibersite and rhabdite, as well as iron-sulfur compounds in the forms of troilite FeS and daubréelite $FeCr_2S_4$. Previously, we have analyzed extracted $(Fe,Ni)_3P$ in both forms using magnetization and Mössbauer spectroscopy [22–24]. In the present work we continue the analysis of iron containing inclusions extracted from the Sikhote-Alin kamacite matrix by focusing our attention on a sample with an extracted troilite inclusion. We present a detailed analysis carried out by using powder X-ray diffractometry (PXRD), scanning electron microscopy (SEM) combined with energy-dispersive X-ray spectroscopy (EDS), magnetization measurements, ferromagnetic resonance spectroscopy and $^{57}Fe$ Mössbauer spectroscopy with a high velocity resolution (with a higher discretization order of the velocity scale). The last-named technique demonstrates significant advances in comparison with conventional Mössbauer spectroscopy in chemical analyses of iron-containing species in materials, cosmochemical and biomedical sciences [25–29].

DOI: 10.1016/j.matchemphys.2016.02.056

## 2. Materials and Methods

By cutting a fragment of Sikhote-Alin IIAB iron meteorite a massive iron sulfide inclusion was found (Fig. 1). This troilite inclusion was mechanically extracted from the kamacite matrix and powdered for further investigation. This powder (with an iron surface density of 10 mg Fe/cm$^2$) was glued on iron-free aluminum foil for Mössbauer measurements. SEM and EDS measurements were performed by ΣIGMA VP microscope (Carl Zeiss) with EDS device X-max (Oxford Instruments). PXRD study was carried out using PANalytical X'pert PRO diffractometer (The Netherlands) with Cu $K_\alpha$ radiation and Ni filter at the Ural Federal University (Ekaterinburg). Measurements were done in the 2Θ range of 17–90° with steps of 0.013° and a step time of 300 s. To minimize the effect of different crystal sizes as well as the texture effect the sample was rotated in horizontal plane with revolution time of 8 s. The observed X-ray diffractograms were fitted with the least squares procedure using the program Panalitical X'Pert High Score Plus (version 2.2c) employing the Rietveld full profile refinements and PDF-2 database. Magnetic measurements were made using commercial SQUID magnetometer MPMS-5S (Quantum Design) at the Hebrew University (Jerusalem).

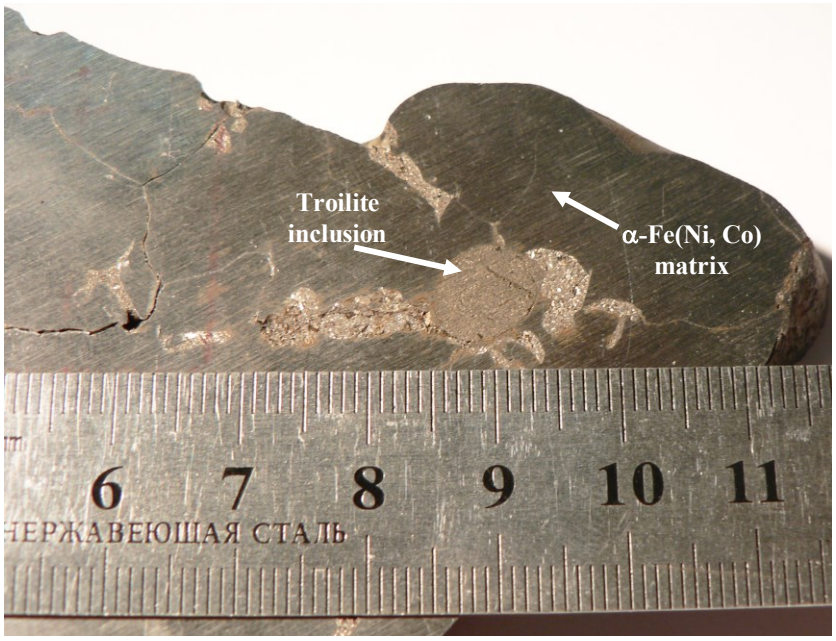


**Fig. 1.** Fragment of the Sikhote-Alin iron meteorite with troilite inclusion.

DOI: 10.1016/j.matchemphys.2016.02.056

Ferromagnetic resonance (FMR) spectroscopy measurements were carried out on 2.3 mg of the powdered sample, by a Bruker ElexSys E500 X-band spectrometer equipped with a variable-temperature flow-through type insert in conjunction with a digital temperature control unit, at the Institute of Materials and Environmental Chemistry (Budapest). Measurements were carried out first (series A) in the range of 320–140 K (by applying evaporated liquid nitrogen as coolant), and subsequently (series B) in the range of 300–550 K. The conditions of FMR measurements involved 2 scans, each with a sweep time of ~84 s, with modulation frequency of 100 kHz, modulation amplitude of 5 G, microwave power of ~2 mW (series A) and ~10 mW (series B), and microwave frequency in the range of 9.33–9.44 GHz. The spectra (being proportional to the first derivative of the power of microwave absorption with respect to the applied magnetic field) were recorded in 2048 channels in the magnetic field range of 200–10800 G. The magnetic field axes of the spectra have been scaled together to the common microwave frequency of 9.338 GHz before processing.

Mössbauer spectra with a high velocity resolution were measured at the Ural Federal University (Ekaterinburg) using an automated precision Mössbauer spectrometric system built on the base of the SM-2201 spectrometer with a saw-tooth shape velocity reference signal formed by the digital-analog convertor using quantification with 4096 steps. Details and characteristics of this spectrometer and the system are given in [28–30]. The $^{57}$Co(Rh) source of about $1.5\times10^{9}$ Bq (Ritverc GmbH, Saint-Petersburg) was used at room temperature. Spectra registered in 4096 channels were measured in transmission geometry with the moving absorber in the liquid nitrogen cryostat either at 295 K or at 90 K. To enable a reliably accurate analysis of the spectra, $1.1\times10^{6}$ and $9.8\times10^{5}$ counts per channel were registered and the signal-to-noise ratios were 122 and 153 for 295 K and 90 K, respectively.

The Mössbauer spectra were analyzed by the MossWinn program by applying the following nuclear constants for the ground ($I_g = 1/2$) and excited ($I_e = 3/2$) nuclear levels of $^{57}$Fe: $g_g = 0.18088$, $g_e = -0.103267$, $Q_e = 0.16$ barn, where $g_g$ and $g_e$ stand, respectively, for the nuclear $g$ factor of the ground and the excited state, and $Q_e$ denotes the quadrupole moment of the excited state. Parameters

DOI: 10.1016/j.matchemphys.2016.02.056

determined for the measured spectra were: isomer shift, δ, main component and asymmetry parameter of the EFG, $V_{zz}$ and η respectively, magnitude of the hyperfine magnetic field $\mathbf{B}_{hf}$, polar β and azimuthal α angles of $\mathbf{B}_{hf}$ in the eigensystem of the EFG, quadrupole splitting, $\Delta = (eQ_e V_{zz}/2)\sqrt{1+\eta^2/3}$ where $e$ is the elementary charge, or the apparent first order quadrupole shift [31], ε, line width (full width at a half maximum) of the individual Lorentzian lines, Γ, and normalized statistical criteria of fitting quality $\chi^2$. As criteria for choosing the best fits, the differential spectrum, $\chi^2$ and a physical meaning of the fit parameters were considered. The instrumental (systematic) error in the Doppler velocity values attributed to the individual spectrum points and to the hyperfine parameters were equivalent to ±0.5 and ±1 channel, respectively [29]. The velocity resolution in the spectra was ~0.0039 mm/s per channel. The relative instrumental error of the spectral/sub-spectral area did not exceed 10 %. In cases when the fit procedure yielded a statistical uncertainty in the derived fit parameters below the instrumental (systematic) error, we quote the latter. All isomer shift values are given relative to that of α-Fe at 295 K.

## 3. Results and Discussion

### *3.1. Characterization of iron sulfide inclusion extracted from Sikhote-Alin iron meteorite by means of scanning electron microscopy, X-ray diffraction and magnetization measurements*

SEM images obtained with different magnifications of troilite inclusion extracted from Sikhote-Alin iron meteorite are shown in Fig. 2a,b. An example of energy dispersion spectrum observed for troilite is shown in Fig. 2c. On the basis of EDS analyses performed at several points in different microcrystals the average chemical composition is: ~34(1) wt.% S, ~65(1) wt.% Fe and ~1 wt.% Cr. (In good agreement with corresponding values expected for stoichiometric FeS: 36.5 wt.% S and 63.5 wt.% Fe). The detected amount of Cr can be attributed to $FeCr_2S_4$ being present as a minority phase (see below).

DOI: 10.1016/j.matchemphys.2016.02.056

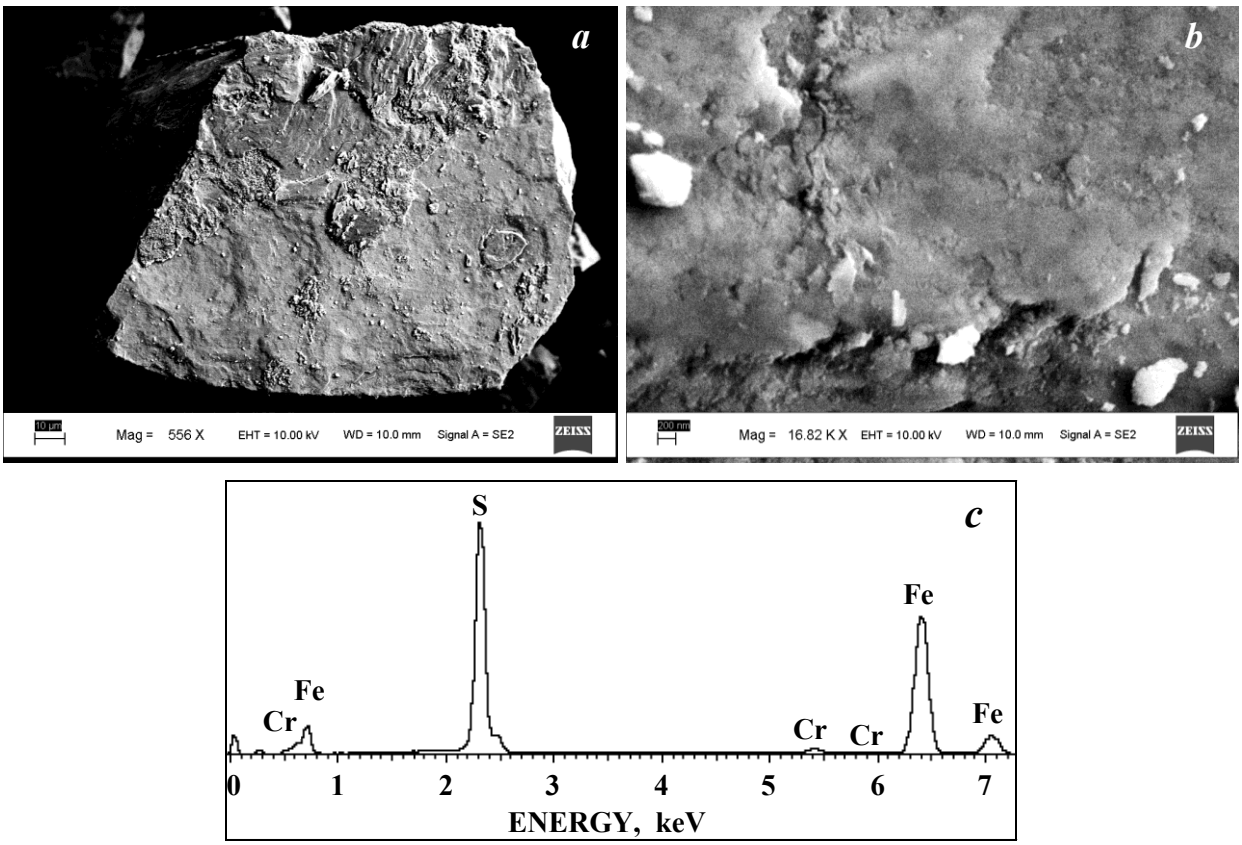


**Fig. 2.** Scanning electron microscopy images of powdered troilite inclusion extracted from Sikhote-Alin iron meteorite with different magnifications, scale bars of 10 μm (***a***) and 200 nm (***b***), and energy-dispersive X-ray spectrum of troilite inclusion (***c***).

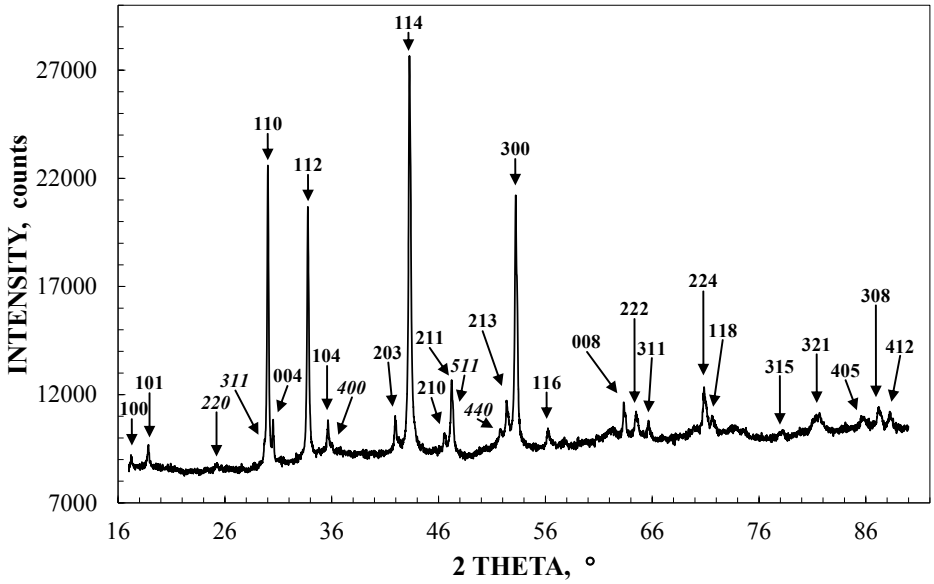


**Fig. 3.** X-ray diffraction patterns of powdered troilite inclusion extracted from Sikhote-Alin iron meteorite, Miller indexes in bold indicate FeS reflections while those in bold italic indicate reflections from $FeCr_2S_4$.

DOI: 10.1016/j.matchemphys.2016.02.056

The X-ray diffraction pattern of the sample is shown in Fig. 3. The Rietveld refinement analysis yields ~93 wt.% of FeS and ~7 wt.% of $FeCr_2S_4$. Within the uncertainties, the corresponding Cr content (~2.5 wt.%) is in fair agreement with the results of EDS analysis. Note, that these compositions are similar to that obtained for the troilite sample extracted from Nantan IAB-MG iron meteorite [32]. It is well known (see [10]) that at low temperatures the hexagonal crystal lattice of troilite can be derived from NiAs structure sub-cell with parameters $A$ and $C$, where the troilite super-cell axes are $a = \sqrt{3}A$ and $c = 2C$. The structural parameters extracted here are: $a = b = 5.9696(8)$ Å, $c = 11.715(6)$ Å and the space group is $P\bar{6}2c$ (see Fig. 4a). It is a non-centrosymmetric structure (like NiAs), which leads to two possible different spatial environments of the constituent atoms inside the unit cell [11]. The XRD pattern of daubréelite is analyzed on the basis of a cubic spinel structure (space group $Fd\bar{3}m$) with: $a = b = c = 9.98(5)$ Å (see Fig. 4b).

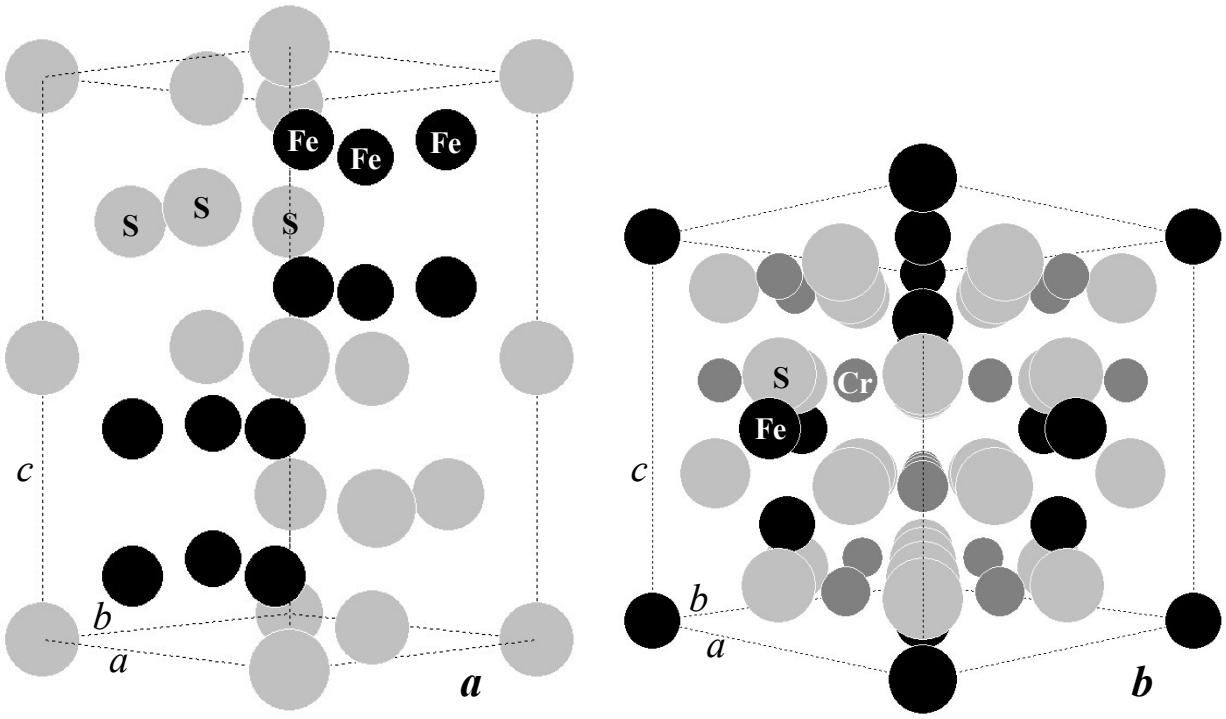


**Fig. 4.** The unit cell structures of troilite (***a***) and daubréelite (***b***) found in troilite inclusion extracted from Sikhote-Alin iron meteorite obtained from the XRD data; ● – Fe, ● – Cr, ● – S, $a$, $b$ and $c$ are the unit cell parameters (see values in the text).

DOI: 10.1016/j.matchemphys.2016.02.056

It is also known that FeS has a tendency to a slight deficiency of cations in its crystal cell. This leads to a distortion of the structure and affects the values of the lattice parameters [9]. The experimental data for synthetic $Fe_{1-x}S$ samples and for natural troilite in a wide range of $x$ were obtained by Kruse [9, 10]. The functional dependence of the cell parameters $a$, $c$ and the $d_{114}$ diffraction peak position as a function of $x$ in $Fe_{1-x}S$ was found to be nearly linear for small $x$ values [9]. The linear dependence of the $d_{114}$ diffraction peak position vs. $x$ (taken from [9]) is shown in Fig. 5. On this basis in the present material $d_{114} = 2.0899(3)$ Å yields $x = 0.0148$. By varying the occupancy of iron in our XRD model by using the Rietveld procedure, we obtain $x = 0.0145$, a value that fits well with the former result.

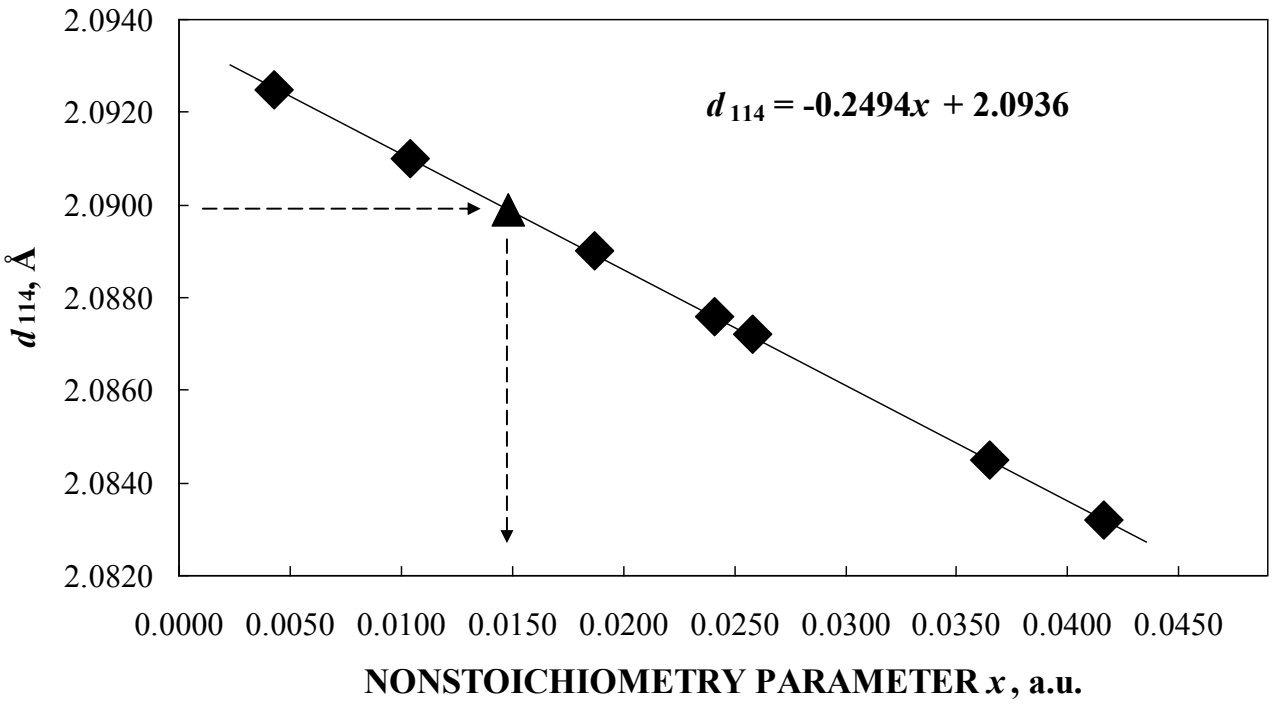


**Fig. 5.** Evaluation of the $x$ degree of non-stoichiometry for troilite extracted from Sikhote-Alin iron meteorite (▲) using the linear dependence of $d_{114}$ diffraction peak position vs. $x$ values (◆) taken from Kruse and Ericsson (1988). Arrows indicate determination of $x$ for troilite in the present study.

DOI: 10.1016/j.matchemphys.2016.02.056

Zero field cooled (ZFC) and field cooled (FC) curves of troilite inclusion measured at 110 Oe are shown in Fig. 6a. The two curves show a distinguished peak at 74 K and sharp magnetic transition at 166(2) K. For ambient conditions, stoichiometric FeS with the troilite crystal structure is antiferromagnetically ordered with $T_N$ of about 600 K [10, 33]. For $0<x<0.15$ the $Fe_{1-x}S$ system crystallize in the troilite structure and becomes antiferromagnetic already above room temperature [33]. Thus, none of the phenomena observed in Fig. 6a belong to the major troilite phase. On the other hand, Mössbauer spectroscopy and magnetic measurements show that $FeCr_2S_4$ is a ferrimagnetic semiconductor, crystallizing in the normal spinel structure (as stated above), with a Curie temperature around 177 K [34]. Therefore it is assumed that Fig. 6a reflects the minority phase 7% $FeCr_2S_4$ (daubréelite) properties which is present in the troilite inclusion. The transition of around 168 K is its ferrimagnetic transition while the peak around 74 K is probably due to a partial reorientation of this ferrimagnetic structure. Similar ZFC and FC plots were also obtained for various $FeCr_2S_4$ crystals [35–37], for $FeCr_2S_4$ bulk samples [38, 39] and for troilite extracted from Nantan IAB-MG iron meteorite [32]. Obviously they differ from plots observed for troilite extracted from Cape York IIIAB iron meteorite which does not contain daubréelite [40].

The isothermal magnetization curves at 5, 150 and 300 K measured up to 15 kOe are shown in Fig. 6b. It is readily observed that saturation is not fully reached even at $T = 300$ K (above the phase transition temperature 168 K). The $M(H)$ curve at 300 K can be fitted as: $M(H) = M_S + (\chi_A+\chi_P)H$, where $M_S$ is the spontaneous ferromagnetic magnetization (~0.74 emu/g) and $(\chi_A+\chi_P)H$ are the linear antiferromagnetic contribution (of FeS) and the paramagnetic intrinsic susceptibility of $FeCr_2S_4$ (above 168 K) respectively all shown in Fig. 6b. The magnetic hysteresis loop observed at 300 K, Fig. 6c, exhibits a coercive field of $H_C = 150$ Oe, revealing soft ferromagnetism in the sample at ambient temperature. The latter is further confirmed by the observation that the two ZFC and FC branches in Fig. 6a do not merge at 168 K, but rather show a tiny irreversibility up to the room temperature.

DOI: 10.1016/j.matchemphys.2016.02.056

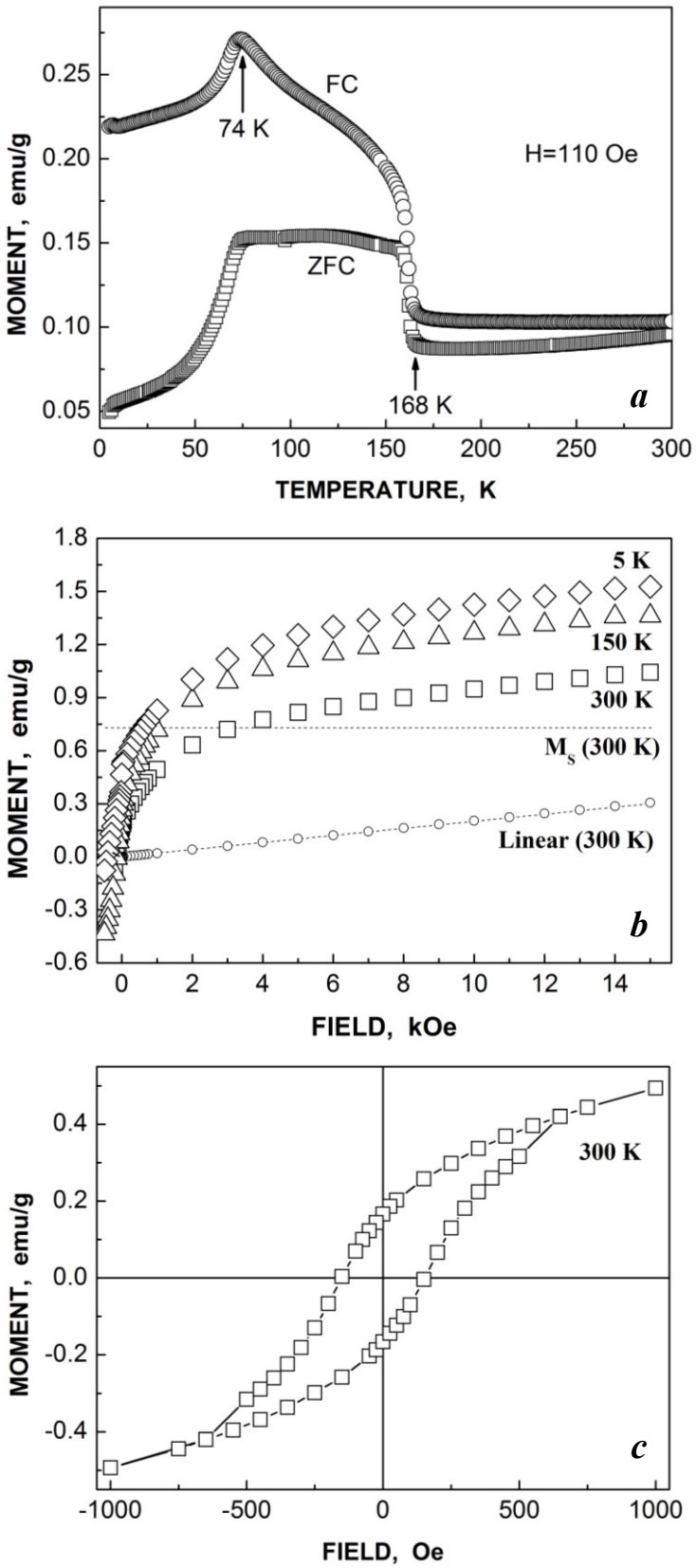


**Fig. 6.** Magnetization measurements of powdered troilite inclusion extracted from Sikhote-Alin iron meteorite: magnetization vs. temperature, ZFC – zero field cooled and FC – field cooled curves (***a***), magnetization vs. magnetic field (***b***) and magnetic hysteresis loop at T = 300 K (***c***).

DOI: 10.1016/j.matchemphys.2016.02.056

The compositional (SEM-EDS), structural (XRD) and bulk magnetic analysis of the present sample thus consistently refer to the presence of daubréelite as a minority phase with a decisive contribution to the sample's bulk magnetization below its Curie temperature of ~168 K. At the same time, the main phase can be identified as troilite with an average non-stoichiometry remaining low at $x \approx 0.0145–0.0148$ in $Fe_{1-x}S$. The spontaneous ferromagnetic magnetization of ~0.74 emu/g detected in the $M(H)$ curve at 300 K is roughly equivalent to ~0.0124 $\mu_B$ per $Fe_{1-x}S$ formula unit, and further to ~0.85 $\mu_B$ average ferromagnetic moment for each iron atom vacancy in $Fe_{1-x}S$. Assuming, as reflected by the XRD pattern, that our sample is composed exclusively from troilite and daubréelite, this small amount of spontaneous ferromagnetic magnetization detected at 300 K may be attributed to magnetism produced by uncompensated iron magnetic moments in non-stoichiometric troilite.

### *3.2. Characterization of iron sulfide inclusion extracted from Sikhote-Alin iron meteorite by ferromagnetic resonance spectroscopy*

FMR spectra of the sample at various temperatures are shown in Fig. 7. In the range of 175–320 K the main feature is a broad ferromagnetic signal whose shape and position show only minor changes with temperature, suggesting that the corresponding magnetic phase (here referred to as phase M) is magnetically ordered well above 320 K. That is consistent with the magnetization data presented in Fig. 6 and reported by Cuda et al. [40]. The signal of daubréelite (being superimposed on the signal of phase M mainly in between 2000 and 6000 G) becomes clearly observable in the FMR spectra (Fig. 7) at its known Curie temperature of $T_c \approx 170$ K [35–37, 41, 42]. The association of the signal in question with $FeCr_2S_4$ is corroborated by the temperature dependence of the signal's peak-to-peak width (i.e. $\Gamma_{pp} = B_{min}–B_{max}$ where $B_{min}$ and $B_{max}$ denote, respectively, the magnetic field belonging to the minimum and the maximum of the corresponding FMR signal part) and that of its $B_0$ center (here defined as $B_0 = (B_{min}+B_{max})/2$), which are depicted in Fig. 8. Namely, $\Gamma_{pp}$ and $B_0$ start to increase with decreasing temperature at around 155 K, where in $FeCr_2S_4$ magnetocrystalline anisotropy [41] and long-range magnetic order (along with associated electric field gradient at the

DOI: 10.1016/j.matchemphys.2016.02.056

iron nuclei) are also expected to set in [42]. Furthermore, the simultaneous increase of $\Gamma_{pp}$ and $B_0$ below 155 K (Fig. 8) suggests increasing levels of positive magnetocrystalline anisotropy [43], as expected for daubréelite [41]. The opposite trend observed for $B_0$ between 155 K and 170 K may be caused by shape anisotropy of the particles [41]. The FMR measurements thus confirm that the increase of sample magnetization detected in our sample at ~166 K (Fig. 6a) can be attributed to daubréelite.

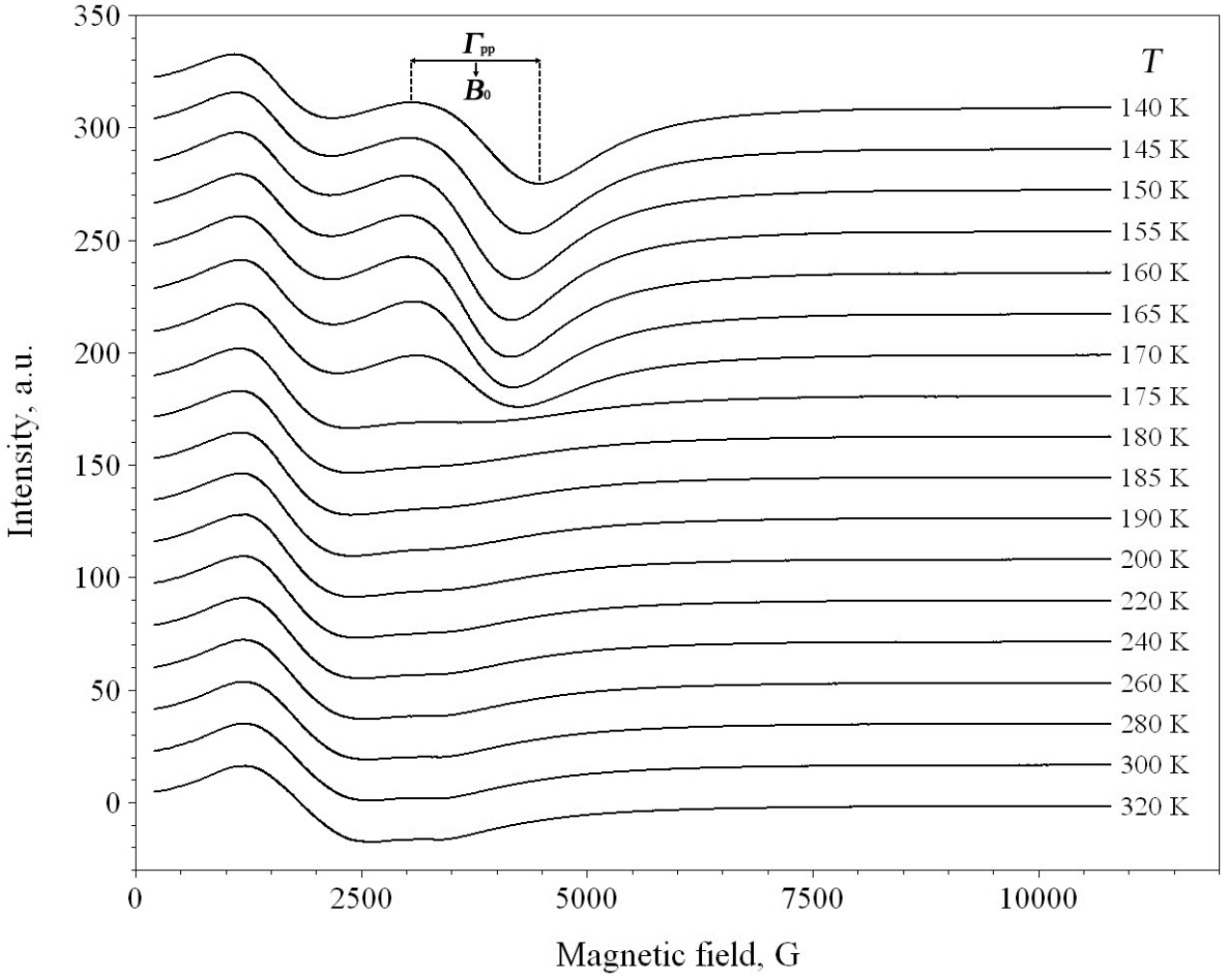


**Fig. 7.** Ferromagnetic resonance spectra (series A) of powdered troilite inclusion extracted from Sikhote-Alin iron meteorite measured at the temperatures indicated right beside the curves. The meaning of the apparent spectrum parameters ($\Gamma_{pp}$ and $B_0$) used to characterize the signal attributed to the $FeCr_2S_4$ phase are indicated on the spectrum measured at $T$ = 140 K. The accuracy of the given temperature values is better than 1 K. The magnetic field axes of the individual measurements are scaled together according to the spectrometer frequency of 9.338 GHz.

DOI: 10.1016/j.matchemphys.2016.02.056

The large width of the signal of phase M can be contributed to by anisotropy broadening expected to be present in powdered samples where the easy magnetization direction(s) of the individual particles are randomly oriented with respect to the sweeping magnetic field of the spectrometer. At the measuring frequency of $f = 9.338$ GHz, at $T = 300$ K the apparent local maximum and the local minima of the FMR signal are positioned at $B_{max}$≈1189 G, $B_{min,1}$≈2608 G and $B_{min,2}$≈3370 G, respectively. On the basis of the relationship $g = hf/\mu_B B$ (where $h$ is the Planck constant and $\mu_B$ denotes the Bohr magneton) these values correspond to the respective spectroscopic splitting factors of $g_{max}$≈5.61, $g_{min,1}$≈2.56 and $g_{min,2}$≈1.98. The full width at half maximum ($\Gamma_{FWHM}$) of the corresponding absorption signal is $\Gamma_{FWHM}$≈2.07 kG.

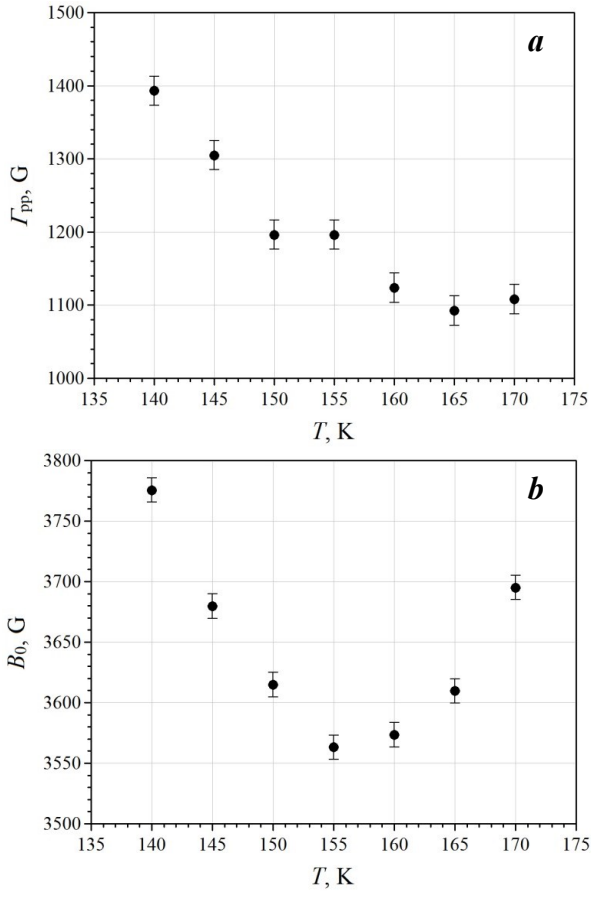


**Fig. 8.** Temperature dependence of the apparent spectrum parameters $\Gamma_{pp}$ (***a***) and $B_0$ (***b***) characterizing the signal of daubréelite detected in the FMR spectra of the sample of troilite inclusion extracted from Sikhote-Alin iron meteorite. See Fig. 7 for the meaning of the depicted parameters. The magnitude of error associated with the depicted data was estimated by assuming 10 G uncertainty in the values of $B_{min}$ and $B_{max}$.

DOI: 10.1016/j.matchemphys.2016.02.056

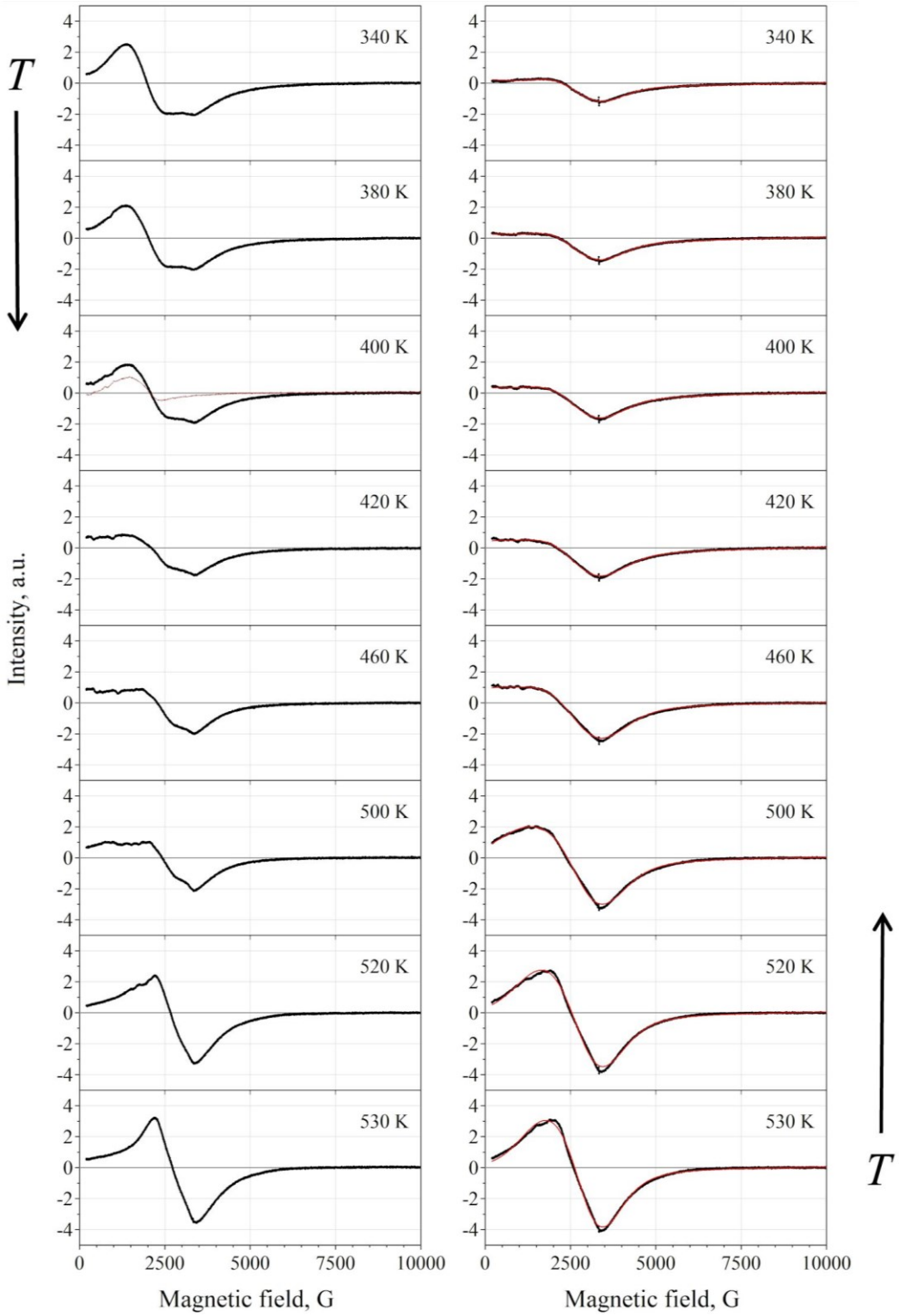


**Fig. 9.** Selected FMR spectra (series B) of the sample of troilite inclusion extracted from Sikhote-Alin iron meteorite measured at temperatures above room temperature during heating (left column) and during subsequent cooling (right column) of the sample up to and down from 555 K. The accuracy of the given temperature values is better than 1 K. The magnetic field axes of the individual measurements are scaled together according to the spectrometer frequency of 9.338 GHz. In the right column the fitting curve is drawn over the data as solid line.

DOI: 10.1016/j.matchemphys.2016.02.056

In order to identify phase M, the FMR signal of the sample was monitored as a function of temperature while heating the sample up to 555 K, and then while cooling it down to 300 K. While the temperature rises from 400 K to 420 K, the spectra reveal a magnetic transition visualized in the loss of considerable signal intensity (Fig. 9). By subtracting the spectrum measured at 420 K from that measured at 400 K we observe the lost signal intensity as depicted in Fig. 9 over the spectrum observed at 400 K. The corresponding signal displays an absorption maximum in the range of $g_0 \approx 3.2–3.3$. Further increase of temperature results in increasing apparent signal intensity, with low-field components gradually merging into a main peak whose asymmetry diminishes with increasing temperature. Spectra recorded during subsequent lowering of the sample temperature to 300 K (Fig. 9) reveal that the transition between 400 K and 420 K is not reversed in the applied range (the minor paramagnetic signal at $g \approx 2$, becoming more prominent on cooling, appears at around 500 K on heating. From the point of view of the present discussion it is not considered to be relevant and will not be dealt with in the followings). The overall spectral shape and the temperature dependence of the apparent signal intensity may be explained by anisotropy broadening of a random powder of magnetic particles with considerable positive magnetocrystalline anisotropy [44]. With decreasing temperature the magnetic anisotropy energy density and the associated effective magnetic anisotropy field ($B_a$) increase, which leads to a gradual decrease of the number of particles that have suitable orientation to contribute to the resonance signal at the applied microwave frequency. In the actual spectra (Fig. 9) this effect is visualized as if with decreasing temperature part of the signal was gradually shifted to negative resonance field values. We found that the spectra observed on cooling are well approximated by assuming anisotropy broadening due to positive cubic magnetocrystalline anisotropy. The corresponding fitting curves (depicted also on Fig. 9) were calculated for a random powder in accordance with Eq. (6) of Griscom [45] by assuming the second- and the third-order anisotropy constants to be zero. The intrinsic peak shape was assumed to be a Voigt function whose Gaussian width was allowed to vary with temperature. The temperature dependence of the effective magnetic anisotropy field, and that of the $g_{eff}$ effective spectroscopic splitting factor (that would

DOI: 10.1016/j.matchemphys.2016.02.056

correspond to the maximum of absorption if $B_a$ was zero), as observed from the fit, are shown in Fig. 10. The anisotropy field tends to decrease with increasing temperature and on the basis of a linear extrapolation (Fig. 9) it goes to zero at ~598 K, which may signal a transition to the paramagnetic state of the corresponding phase. The effective spectroscopic splitting factor appears to approach its paramagnetic limit (~2) at around the same temperature.

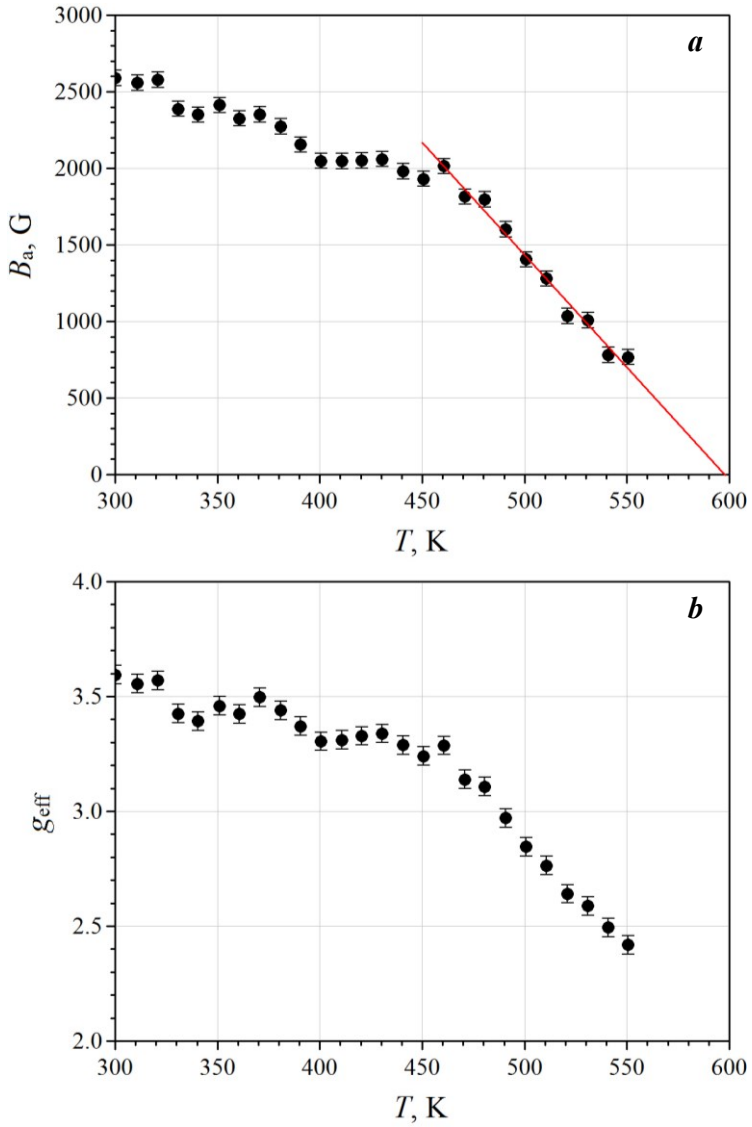


**Fig. 10.** Effective magnetic anisotropy field (top), and the effective spectroscopic splitting factor (bottom), derived on the basis of the FMR spectra (Fig. 9) observed while cooling the sample of troilite inclusion extracted from Sikhote-Alin iron meteorite from 550 K to 300 K. The line through the points in the upper graph reflects the result of a linear fit to the data observed for $T \geq 470$ K. The fitting curves shown for the selected spectra in Fig. 9 correspond to the data shown here for the respective temperatures.

DOI: 10.1016/j.matchemphys.2016.02.056

On the basis of the magnetic transition temperatures determined for phase M above room temperature, it may be identified as troilite proper with slight iron deficiency and corresponding magnetization. Namely, the temperature region 400–420 K where part of the signal intensity was lost on heating fits well to the range of $T_\alpha$ transition temperatures reported for the α transition of troilite to the orthorhombic MnP-type structure [10, 46]. The absorption maximum of the lost signal also occurs at a *g* factor close to that found for pyrrhotite (~3.1) [46, 47]. The estimated paramagnetic transition temperature (Fig. 9) also agrees well with the known Néel temperature of troilite $T_N \approx 600$ K [10, 33].

A further increase in temperature above $T_\alpha$ leads to another marked change of the FMR signal shape (Fig. 9) between 500 and 520 K, which may be the consequence of the structural transition of troilite from the orthorhombic MnP-structure to the hexagonal NiAs-structure, for which a transition temperature in the range of ~483–508 K was reported by Kruse and Ericsson [8] and Kruse [9]. However, on cooling the same transition occurs in the opposite direction at lower temperatures, between 500 K and 460 K (Fig. 9). This kind of hysteretic behavior is in correspondence with the observation of a range of temperature values for the NiAs-structure ↔ MnP-structure first-order phase transition in troilite [10].

As mentioned before, the observed change in the FMR signal attributed to the α transition in the range of 400–420 K during heating of the sample is not reversed on cooling (Fig. 9). This behavior may reflect that on cooling the phase with the MnP-type structure can survive well below $T_\alpha$ similarly to corresponding observations reported by Kruse and Ericsson [8]. At the same time, the signal loss on heating through the range of 400–420 K may also be connected to an irreversible antiferromagnetic pairing of previously uncompensated iron spins as a consequence of the α transition of troilite.

Ferromagnetic resonance spectroscopy thus provides further evidence for the presence of at least two different magnetic phases in our sample. One is clearly identified as daubréelite whose

DOI: 10.1016/j.matchemphys.2016.02.056

contribution to the FMR signal becomes detectable below its Curie temperature. Another magnetic phase displays magnetic transitions with characteristic transition temperatures that coincide with known phase transition temperatures of troilite. Given that stoichiometric troilite is antiferromagnetic and is therefore expected to be FMR-silent in our experiments, we can attribute the appearance of the corresponding FMR signal to non-stoichiometric troilite in agreement with the hypothesis put forward regarding the origin of the spontaneous ferromagnetic magnetization detected at 300 K (Fig. 6b). It is therefore plausible to suppose that spontaneous magnetism detected at room temperature in our extracted sample is governed by the non-stoichiometry of troilite.

### *3.3. Mössbauer spectroscopy of iron sulfide inclusion extracted from Sikhote-Alin iron meteorite*

The $^{57}$Fe Mössbauer spectra of the sample measured at temperatures of 295 K and 90 K are shown in Fig. 11. The spectra are dominated by a sextet of intense peaks due to iron in the troilite proper. In addition, minority spectrum components reveal themselves partly via the broad inward shoulders of the six intense peaks, and partly via additional signal intensity in and around the velocity range from 0 to 1 mm/s in the spectrum recorded at 295 K.

Here we attempt to analyze the spectrum of troilite inclusion in two steps, which constitutes a novel approach. In the first step we apply essential approximations that include the assumptions that (1) the shape of the individual absorption peaks is Lorentzian (the line shape of the standard absorber α-Fe Mössbauer spectrum is pure Lorentzian, which proves that the experimental conditions allow to use this supposition), and that (2) the spectrum can be composed as the sum of the various spectral components originating from the $^{57}$Fe nuclei in different microenvironments. On this basis we wish to extract the main spectrum component characteristic of troilite by accounting for additional signals in a quasi model-independent way, and then fit the extracted spectrum component of troilite separately to a full Hamiltonian pattern [48] in order to derive its Mössbauer parameters. During the extraction step, the spectrum component of troilite is assumed to be accounted for by 8 Lorentzian

DOI: 10.1016/j.matchemphys.2016.02.056

singlets with unrestricted positions and amplitudes but with pairwise equal line widths for the 1st–6th, 2nd–5th, 3rd–4th in conventional sextet and additional two low-intensity 7th–8th lines [48].

The position of these low-intensity lines (appearing due to the mixing of the $^{57}$Fe excited state nuclear sublevels by the electric quadrupole interaction) can be readily estimated in advance by a rough fit to a full Hamiltonian pattern. At 295 K they arise at around velocities of −0.70 mm/s and 2.06 mm/s, and altogether account only for ~0.53 % of the intensity of the correspondent subcomponent. A further singlet spectrum component was used to fit the small peak at ~0.65 mm/s that represents the presence of $FeCr_2S_4$ in the sample.

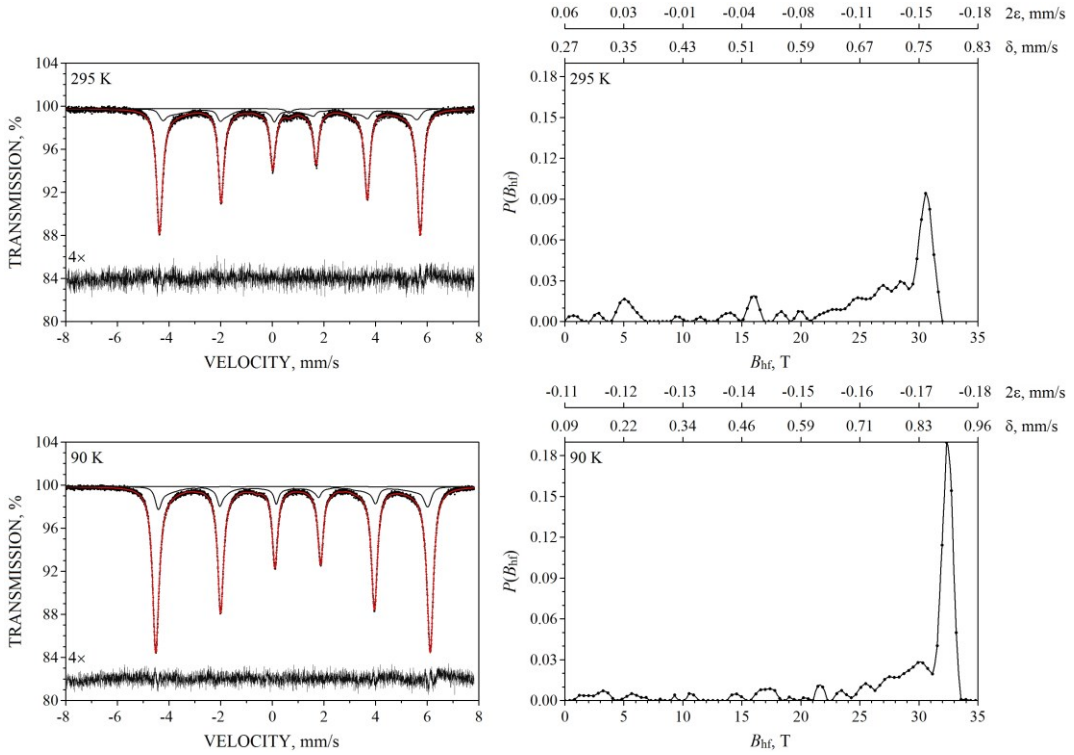


**Fig. 11.** The $^{57}$Fe Mössbauer spectra and corresponding fit envelopes (drawn with solid line) and differential spectra (magnified by a factor of 4 for clarity) of the powdered troilite inclusion extracted from Sikhote-Alin iron meteorite measured at 295 K and 90 K (left column) in 4096 channels, and the respective (formal) hyperfine magnetic field distributions (right column) resulting in the minor magnetic subspectrum envelope also shown on the left-side images. The scale of the δ isomer shift and that of 2ε drawn (rounded to 2 decimals) on the top of the distribution graphs characterize the linear correlation of δ and 2ε with the hyperfine magnetic field as observed for the best fit. Note that the individual envelopes of the 8 Lorentzians accounting for the main iron microenvironment in troilite are omitted on the left-side images for clarity; their contribution is depicted in Fig. 12.

DOI: 10.1016/j.matchemphys.2016.02.056

The rest of the spectral area was fitted according to a hyperfine magnetic field distribution of magnetically split sextet components calculated for 90 different hyperfine magnetic field values distributed equidistantly in the magnetic field range of 0–32 T. For these sextet components linear correlation was assumed to exist between the hyperfine magnetic field and the isomer shift and quadrupole splitting – here treated as to be equal to 2ε [31] – parameter values. The spectrum measured at 90 K was described in a similar way, with the difference that the presence of $FeCr_2S_4$ was accounted for by a sextet component instead of a singlet, and the known parameters [42] and the line width of the latter component were fixed during the fit. As depicted in Fig. 11, during this extraction step a near perfect fit of the spectra could be achieved, with the normalized $\chi^2$ being equal to 1.047 (for 295 K) and 1.157 (for 90 K). The observed distributions reveal components with 29–33 T hyperfine magnetic field and corresponding isomer shift and quadrupole splitting (2ε) values that are very similar to those expected for troilite, and can be identified as to originate from minority components related to iron with nearby iron vacancies in $Fe_{1-x}S$ [9] in agreement with the finite non-stoichiometry evaluated for the present sample. The remaining parts of the distributions are expected to account for the signal of minority chalcogenide spinel components. These can be magnetic sextet as well as doublet components as it was found for these compounds earlier [49–53]. In particular, we note that the minor component reflected by the distribution at ~5 T field for the 295 K spectrum (Fig. 11) can account (approximately) for one or more doublet components for example. The main troilite component (accounting for ~78.3(2) % and ~80.0(1) % of the total spectral area at 295 K and 90 K, respectively) was extracted by subtracting the fit envelope of the rest of the fitted components from the measured spectra. It is plausible to assume that this component represents the majority of iron microenvironments in $Fe_{1-x}S$ that is analogous to the iron microenvironment in FeS. Consequently, the main phase of inclusion is troilite with iron atoms being present with microenvironment corresponding dominantly to stoichiometric FeS while remaining amount of iron atoms in troilite can be associated with microenvironments corresponding to non-stoichiometric $Fe_{1-x}S$.

DOI: 10.1016/j.matchemphys.2016.02.056

In the second step of the Mössbauer spectral analysis the residual troilite spectra obtained in the first step (Fig. 12) were fitted by an octet of peaks whose relative positions and intensities were calculated on the basis of the direct diagonalization of the nuclear Hamiltonian (D.D.H.) accounting for the combined effect of hyperfine magnetic and electric quadrupole interactions. During the fits the asymmetry parameter of the EFG was fixed arbitrarily to 0.3 for both spectra, on one hand, to avoid the ambiguity problem concerning the remaining hyperfine parameters of $V_{zz}$, β, and α and, on the other hand, to enable straightforward comparison of the observed results with earlier observations by Grandjean et al. [13]. By assuming that the sample geometry is that of a perfect powder, the analysis of the spectra (Fig. 12) resulted in the fit parameters listed in Table 1. For the sake of comparison we have also fitted the extracted spectra of Fig. 12 to sextets by applying the usual first-order approximation method (F.O.A.) [31] with the relative intensity of the 2$^{nd}$ and 5$^{th}$ lines treated as a free parameter. The corresponding best fitting curves and differential spectra are shown in Fig. 12, whereas the obtained fit parameters are also listed in Table 1.

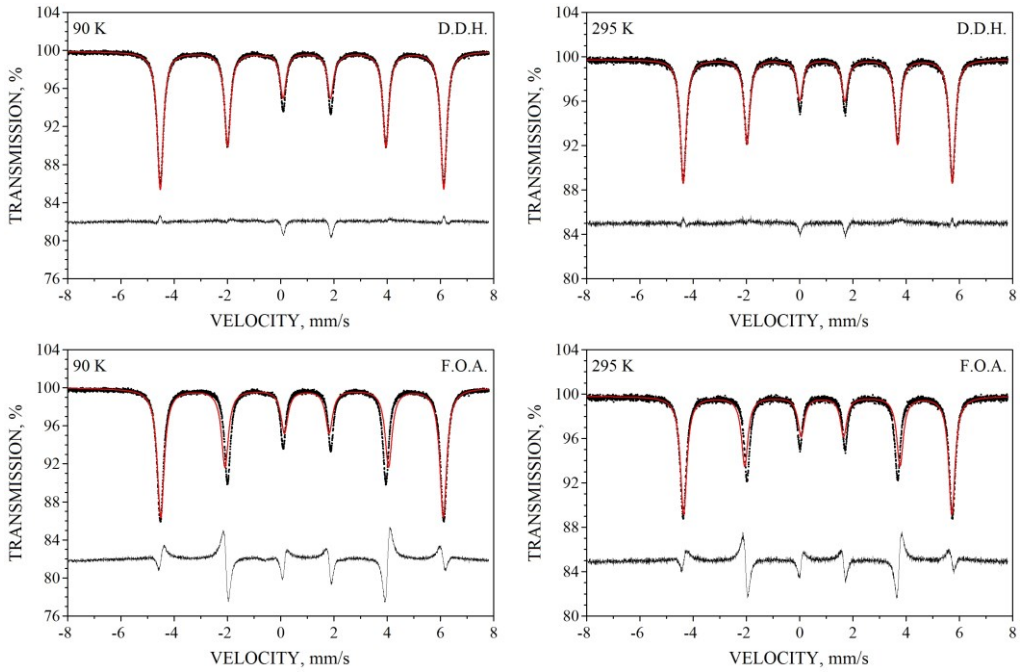


**Fig. 12.** The $^{57}$Fe Mössbauer spectrum component (extracted from the measured spectra shown in Fig. 11 as described in the text) characterizing the main microenvironment of iron in troilite at 90 K and 295 K, and corresponding best fitting curves achievable via the direct diagonalization of the nuclear hyperfine Hamiltonian (D.D.H., top), and via the usual first order approximation (F.O.A., bottom). The differential spectra are shown below the spectra.

DOI: 10.1016/j.matchemphys.2016.02.056

Clearly, the applied method was able to extract the 8 independent Lorentzians at their correct positions, as they can be fitted quite well via the D.D.H. method by assuming a single iron microenvironment only. At the same time, the F.O.A. method is unable to properly account for the position of the lines (Fig. 12), which is in accordance with the expectations and underlines the ability of the applied extraction method to yield the correct line positions for the main troilite spectral component. The latter is further confirmed by the δ and $B_{hf}$ values obtained via the D.D.H. method, which agree well with corresponding values observed by Kruse and Ericsson [8] and Grandjean et al. [13]. However, the magnitude of quadrupole splitting (Δ) observed at 295 K exceeds that reported in [13] (taking into account the factor $\sqrt{1+\eta^2/3}$), and in contrast with [13] we clearly observe a temperature dependence of Δ, similarly to [8]). The observed Δ values for 295 K (Table 1) as well as for 90 K are in excellent agreement with results reported by Kruse and Ericsson (1988) for troilite extracted from the Cape York (Agpalilik) IIIAB iron meteorite.

At room temperature we observe polar and azimuthal angles of the $\mathbf{B}_{hf}$ in the eigensystem of the EFG that slightly differ from those found by Kruse and Ericsson [8] and Grandjean et al. [13]. The angles β and α are strongly correlated fit parameters, so that in our case the increase of angle α (compared to [8] and [13]) may in part be connected to the decrease of angle β.

While the simpler F.O.A. approach can still provide the value of the isomer shift quite accurately, it can lead to small deviations in the hyperfine magnetic field as reflected by the corresponding data in Table 1. At the same time, due to the inability of the first-order approximation method to reproduce the correct positions of the absorption peaks of FeS, the application of this simpler model of troilite for the decomposition of complex spectra (e.g., of ordinary chondrites including troilite) could also lead to larger errors in the parameters determined for the additional iron-bearing phases being present in the sample.

DOI: 10.1016/j.matchemphys.2016.02.056

**Table 1.** The $^{57}$Fe Mössbauer parameters derived by fitting the extracted spectra of troilite to different fit models (Fig. 12) in each case assuming a single microenvironment of iron. $I_{2,5}/I_{3,4}$ is the relative intensity of the 2nd and the 5th peaks with respect to that of the 3rd and the 4th peaks fitted in the method of F.O.A., $S_0$, $S_1$, and $S_2$ are the invariants whose meaning and calculation are described in [54–56]. Standard deviations (StD) resulting from the fit are given in parentheses. When the StD turned out to be negligible compared to instrumental (systematic) error only the relevant numbers are given without the StD. The value of η was fixed during the fits.

| Temperature | 90 K | | 295 K | |
|---|---|---|---|---|
| Method of analysis | D.D.H. | F.O.A. | D.D.H. | F.O.A. |
| $\chi^2_n$ | 5.31 | 71.93 | 2.12 | 20.47 |
| δ, mm/s | 0.890 | 0.891 | 0.766 | 0.767 |
| $B_{hf}$, T | 32.6 | 33.0 | 31.0 | 31.3 |
| $V_{zz}$, $10^{21}\times$V/m$^2$ | −5.54(3) | | −5.02(4) | |
| η | 0.3 | | 0.3 | |
| β, ° | 46.46(13) | | 45.6(3) | |
| α, ° | 47(1) | | 51.1(2.1) | |
| $I_{2,5}/I_{3,4}$ | | 1.80 | | 1.75 |
| Γ, mm/s | 0.272 | 0.313 | 0.259 | 0.293 |
| Δ, mm/s | −0.935(4) | | −0.85(1) | |
| 2ε, mm/s | | −0.18 | | −0.17 |
| $S_0$, mm/s | 2.29(1) | | 2.08(2) | |
| $S_1$, mm/s | −0.38(1) | | −0.36(2) | |
| $S_2$, mm/s | 1.46(1) | | 1.34(2) | |

DOI: 10.1016/j.matchemphys.2016.02.056

For instance, in the Mössbauer spectra of ordinary chondrites the area of magnetic spectral component(s) of the metal phase is smaller than that of the main paramagnetic spectral components related to silicate phases, while it is comparable with the area of magnetic spectral component related to troilite. Moreover, some peaks of both magnetic sextets appear to be overlapped in the spectra (see [14–21]), which can lead to an increase in the correlation between Mössbauer parameters of both magnetic phases. Therefore, a correct fit of troilite component in this case may help reach better fit of metal phase component(s) in Mössbauer spectra of ordinary chondrites as well.

Table 1 also displays the observed values of the $S_{0,1,2}$ invariants that – when considered together with the value of $B_{hf}$ – unequivocally characterize the relative peak positions in the fitted curve as described by Satuła et al. [54] and Szymański et al. [55], and facilitate more straightforward comparison with related results. Namely, the characterization of the $^{57}$Fe hyperfine interactions in troilite via $\delta$, $B_{hf}$ and the $S_0$, $S_1$, $S_2$ invariants eliminates the ambiguities related to the correlations among the parameters of $V_{zz}$, $\eta$, $\beta$, and $\alpha$, and thereby may contribute to the development of a meaningful classification of the corresponding experimental results obtained for troilite samples from meteorites with different origin as well as from any other extraterrestrial (planetary and asteroid) matter. It is worth to note that the definition of the invariant $S_0$ is particularly simple: it is just $\sqrt{6}$ times the absolute value of the quadrupole splitting.

As for the present case, it is interesting to note that the $^{57}$Fe hyperfine interaction parameters derived for the iron microenvironment associated with that in troilite proper in our sample extracted from the Sikhote-Alin IIAB iron meteorite are found to be in good agreement with corresponding results observed for the Cape York (Agpalilik) IIIAB iron meteorite [8], but regarding the quadrupole splitting parameter it displays a marked difference in comparison with corresponding results obtained for the Jilin meteorite that belongs to the class of H5-type ordinary chondrites [13]. This observation indeed appears to support the hypothesis that the quadrupole splitting (or alternatively the related $S_0$ invariant) – characterizing iron located in the majority microenvironment in troilite –

DOI: 10.1016/j.matchemphys.2016.02.056

may be a suitable parameter for the establishment of a classification scheme of associated extra-terrestrial matter. Corresponding differences between majority iron microenvironments in troilite may be attributed to different effects of the iron vacancy structure (i.e. magnitude $x$ and distribution of iron vacancies in the lattice of $Fe_{1-x}S$) on the hyperfine parameters detected for $^{57}Fe$ nuclei at the main iron microenvironment. On one hand these may be rooted in the effect of non-stoichiometry on the crystal lattice (see [9] and Fig. 5). On the other hand, an evidence of the presence of itinerant electrons in natural troilite was found by Skinner et al. [57]. These electrons may also promote the delocalization of the effects of iron vacancies. Consequently, vacancies may have an influence over bulk regions of the specimen, altering the valence and/or ligand contributions to the electric field gradient at numerous $^{57}Fe$ nuclei in a similar manner, even in the case of $^{57}Fe$ nuclei associated with the main (ideal stoichiometric) microenvironment. Thus, this effect may be visualized in troilite samples from different natural extraterrestrial matter (planets, asteroids and meteorites) as a variation in the quadrupole splitting observed for the main iron microenvironment, provided that the concentration of vacancies varies depending on the origin and thermal history of troilite.

## 4. Conclusion

The sample of iron sulfide (troilite) inclusion extracted from Sikhote-Alin IIAB iron meteorite was characterized in detail by using several complementary techniques including SEM with EDS, XRD, magnetization measurements, FMR and $^{57}Fe$ Mössbauer spectroscopy with a high velocity resolution. EDS indicated the presence of Cr besides Fe and S in the sample. XRD study detected the presence of ~7 wt.% of daubréelite, determined cell parameters of troilite from Sikhote-Alin iron meteorite ($a = b = 5.9696(8)$ Å and $c = 11.715(6)$ Å) and the parameter of non-stoichiometry for $Fe_{1-x}S$ ($x = 0.0148–0.0145$). Magnetization measurements demonstrated two transition temperatures at 168 K and 74 K, both related to magnetic phase transitions of daubréelite. Ferromagnetic resonance spectra of the sample revealed signals related to daubréelite as well as signals that were associated with non-stoichiometric troilite. The temperature dependence of the FMR signal shape revealed hysteretic behavior and magnetic transitions that could be identified as high-temperature structural

DOI: 10.1016/j.matchemphys.2016.02.056

phase transitions of troilite. The $^{57}$Fe Mössbauer spectra of the sample of troilite inclusion measured at 295 and 90 K reflected the presence of minor amounts of daubréelite, iron microenvironments associated with slightly iron deficient $Fe_{1-x}S$, and the main iron microenvironment that is analogous to the microenvironment of iron in stoichiometric FeS. The latter spectrum component was successfully extracted from the measured $^{57}$Fe Mössbauer spectra, and the corresponding hyperfine parameters were determined in a subsequent fit by taking into account the orientation of the hyperfine magnetic field in the eigensystem of the electric field gradient at the $^{57}$Fe nucleus. The $^{57}$Fe hyperfine parameters obtained for the main iron microenvironment in troilite extracted from Sikhote-Alin IIAB iron meteorite were in good agreement with those observed earlier for troilite extracted from Cape York (Agpalilik) IIIAB iron meteorite by Kruse and Ericsson [8], but concerning the quadrupole splitting displayed differences in comparison with results obtained for troilite in the bulk samples of Jilin H5 ordinary chondrite by Grandjean et al. [13]. The differences in the quadrupole splitting as can be found for troilite from different meteorites may be a result of corresponding variations in troilite non-stoichiometry that can affect the electronic and crystal structure and finally lead to the change in the electric field gradient at the $^{57}$Fe nucleus.

The variations concerning the characteristic $^{57}$Fe hyperfine interaction parameters in various troilite samples originating from different meteorites need yet to be analyzed in detail systematically for a wide selection of samples in order to elucidate whether the variations in question can refer to the origin of the extraterrestrial substance (planetary, asteroid or meteoritic) in relation to its chemical composition, formation in the space, thermal (cooling rates and possible reheating) and impact history, etc. It is suggested that beside the parameters $\delta$ and $B_{hf}$ the invariants $S_0$, $S_1$, $S_2$ (rather than the parameters $V_{zz}$, $\eta$, $\beta$, and $\alpha$) should form the basis of the systematic physical chemistry analysis in question. On the basis of the present results the $S_0$ invariant (being proportional to $|\Delta|$) appears to be the most promising candidate to investigate in order to elucidate interdependences between $^{57}$Fe hyperfine interaction parameters in iron sulfide and the origin of its host material.

DOI: 10.1016/j.matchemphys.2016.02.056

## Acknowledgement

The authors wish to thank G.A. Yakovlev (Ural Federal University) for SEM with EDS measurements using Carl Zeiss equipment. This work was supported in part by the basic financing of the Ministry of Education and Science of Russian Federation. A.A.M. is supported in part by the Ural Federal University development program for the young scientists' financial support. This work was carried out within the Agreement of Cooperation between the Ural Federal University (Ekaterinburg) and the Eötvös Loránd University (Budapest).

DOI: 10.1016/j.matchemphys.2016.02.056

## REFERENCES

1. J.W. Anthony, R.A. Bideaux, K.W. Bladh, M.C. Nichols, Handbook of Mineralogy. Vol. 1. Elements, Sulfides, Sulfosalts. Mineral Data Publishing, Tucson, Arizona, 1990.

2. A.J. Brearley, R.H. Jones, Chondritic meteorites. In Planetary Materials (ed. J.J. Papike). 36, Reviews in Mineralogy, Mineralogical Society of America, Chantilly, Virginia, 1998, pp. 3-1–3-398.

3. V.F. Buchwald, Handbook of iron meteorites. Vol. 1: Iron Meteorites in General, University of California Press, Berkeley, 1975.

4. F.J.M. Rietmeijer, Interplanetary dust particles. In Planetary Materials (ed.J.J. Papike), 36, Reviews in Mineralogy, Mineralogical Society of America, Chantilly, Virginia, 1998, pp. 2-29–2-95.

5. J. Garcia-Guinea, L. Tormo, A.R. Ordoñez, O. Garcia-Moreno, Non-destructive analyses on a meteorite fragment that fell in the Madrid city centre in 1896, Talanta 114 (2013) 152–159.

6. J.I. Goldstein, E.R.D. Scott, N.L. Chabot, Iron meteorites: Crystallization, thermal history, parent bodies, and origin, Chem. Erde 69 (2009) 293–325.

7. S. Hafner, M. Kalvius, The Mössbauer resonance of $^{57}Fe$ in troilite (FeS) and pyrrhotite ($Fe_{0.88}S$), Z. Kristal. 123 (1966) 443–458.

8. O. Kruse, T. Ericsson, A Mössbauer Investigation of Natural Troilite from the Agpalilik Meteorite, Phys. Chem. Minerals 15 (1988) 509–513.

9. O. Kruse, Mössbauer and X-ray study of the effects of vacancy concentration in synthetic hexagonal pyrrhotites, Am. Mineral. 75 (1990) 755–763.

10. O. Kruse, Phase transitions and kinetics in natural FeS measured by X-ray diffraction and Mössbauer spectroscopy at elevated temperatures, Am. Mineral. 77 (1992) 391–398.

11. R. Skála, I. Císařová, M. Drábek, Inversion twinning in troilite, Am. Mineral. 91 (2006) 917–921.

12. R.A. Dunlap, A Mössbauer effect investigation of the enstatite chondrite from Abee, Canada, Hyperfine Interact. 110 (1997) 209–215.

13. F. Grandjean, G.J. Long, D. Hautot, D.L. Whitney, A Mössbauer spectral study of the Jilin meteorite, Hyperfine Interact. 116 (1998) 105–115.

14. B.S. Paliwal, R.P. Tripathi, H.C. Verma, S.K. Sharma, Classification of the Didwana-Rajod meteorite: a Mössbauer spectroscopic study, Meteorit. Planet. Sci. 35 (2000) 639–642.

15. H.C. Verma, A. Rawat, B.S. Paliwal, R.P. Tripathi, Mössbauer spectroscopic studies of an oxidized ordinary chondrite fallen at Itawa-Bhopji, India, Hyperfine Interact. 142 (2002) 643–652.

16. S.D. Forder, P.A. Bland, J. Galazka-Friedman, M. Urbanski, Z. Gontarz, M. Milczarek, N. Bakun–Czubarow, A Mössbauer study of meteorites – A possible criterion to identify meteorites from the same parent body? Hyperfine Interact. C 5 (2002) 405–408.

17. A.M. Gismelseed, S. Bashir, M.A. Worthing, A.A. Yousif, M.E. Elzain, A.D. Al-Rawas, H.M. Widatallah, Studies and characterizations of the Al Zarnkh meteorite, Meteorit. Planet. Sci. 40 (2005) 255–259.

18. A.D. Al-Rawas, A.M. Gismelseed, A.A. Yousif, M.E. Elzain, M.A. Worthing, A. Al-Kathiri, E. Gnos, B.A. Hofmann, D.A. Steele, Studies on Uruq al Hadd meteorite, Planet. Space Sci. 55 (2007) 859–863.

19. A.D. Al-Rawas, A.M. Gismelseed, A.F. Al-Kathiri, M.E. Elzain, A.A. Yousif, S.B. Al-Kathiri, H.M. Widatallah, S.B. Abdalla, Characterization of Maghsail meteorite from Oman by Mössbauer spectroscopy, X-ray diffraction and petrographic microscopy, Hyperfine Interact. 186 (2008) 105–111.

20. M.I. Oshtrakh, E.V. Petrova, V.I. Grokhovsky, V.A. Semionkin, A Study of Ordinary Chondrites by Mössbauer Spectroscopy with High-Velocity Resolution, Meteorit. Planet. Sci. 43 (2008) 941–958.

21. J.M. Cadogan, L. Rebbouh, J.V.J. Mills, P.A. Bland, An $^{57}$Fe Mössbauer study of three Australian L5 ordinary-chondrite meteorites: dating Kinclaven–001. Hyperfine Interact. 222 (Suppl. 2) (2013) S91–S98.

22. M.I. Oshtrakh, M.Yu. Larionov, V.I. Grokhovsky, V.A. Semionkin, temperature dependent high velocity resolution Mössbauer spectroscopic study of iron nickel phosphide microcrystals (rhabdites) extracted from Sikhote-Alin iron meteorite, J. Alloys Comp. 509 (2011) 1781–1784.

23. M.I. Oshtrakh, M.Yu. Larionov, V.I. Grokhovsky, V.A. Semionkin, An analysis of Fe and Ni distribution in M1, M2 and M3 sites of iron nickel phosphides extracted from Sikhote-Alin meteorite using Mössbauer spectroscopy with a high velocity resolution, J. Mol. Struct. 993 (2011) 38–42.

24. M.I. Oshtrakh, M.Yu. Larionov, V.I. Grokhovsky, V.A. Semionkin, Study of rhabdite (iron nickel phosphide) microcrystals extracted from Sikhote-Alin iron meteorite by magnetization measurements and Mössbauer spectroscopy, Mat. Chem. Phys. 130 (2011) 373–380.

25. M.I. Oshtrakh, V.A. Semionkin, V.I. Grokhovsky, O.B. Milder, E.G. Novikov, Mössbauer spectroscopy with high velocity resolution: new possibilities of chemical analysis in material science and biomedical research, J. Radioanal. Nucl. Chem. 279 (2009) 833–846.

26. V.I. Grokhovsky, M.I. Oshtrakh, E.V. Petrova, M.Yu. Larionov, K.A. Uymina, V.A. Semionkin, Mössbauer spectroscopy with high velocity resolution in the study of iron-bearing minerals in meteorites, Eur. J. Mineral. 21 (2009) 51–63.

27. M.I. Oshtrakh, V.A. Semionkin, O.B. Milder, E.G. Novikov, Mössbauer spectroscopy with high velocity resolution: new possibilities in biomedical research, J. Mol. Struct., 2009, 924–926, 20–26.

28. M.I. Oshtrakh, V.A. Semionkin, O.B. Milder, E.G. Novikov, Mössbauer spectroscopy with high velocity resolution: an increase of analytical possibilities in biomedical research, J. Radioanal. Nucl. Chem. 281 (2009) 63–67.

29. M.I. Oshtrakh, V.A. Semionkin, Mössbauer spectroscopy with a high velocity resolution: advances in biomedical, pharmaceutical, cosmochemical and nanotechnological research. Spectrochim. Acta, Part A: Molec. and Biomolec. Spectroscopy 100 (2013) 78–87.

30. V.A. Semionkin, M.I. Oshtrakh, O.B. Milder, E.G. Novikov, A high velocity resolution Mössbauer spectrometric system for biomedical research, Bull. Rus. Acad. Sci.: Phys. 74 (2010) 416–420.

31. P. Gütlich, E. Bill, A.X. Trautwein, Mössbauer Spectroscopy and Transition Metal Chemistry, Springer-Verlag, Berlin – Heidelberg, 2011.

32. J. Cuda, T. Kohout, J. Tucek, J. Filip, I. Medrík, M. Mashlan, R. Zboril, Mössbauer study and magnetic measurement of troilite extract from Natan iron meteorite. In: Mössbauer Spectroscopy in Materials Science – 2012. AIP Conf. Proc. 1489, 2012, pp. 145–153.

33. J.L. Horwood, M.G. Townsend, A.H. Webster, Magnetic susceptibility of single-crystal $Fe_{1-x}S$, J. Solid State Chem. 17 (1976) 35–42.

34. J.Y. Park, K.J. Kim, Magnetotransport and magnetic properties of sulfospinels $Zn_xFe_{1-x}Cr_2S_4$, Hyperfine Interact. 169 1(2006) 267–1272.

DOI: 10.1016/j.matchemphys.2016.02.056

35. V. Tsurkan, J. Groza, G. Bocelli, D. Samusi, P. Petrenco, V. Zestrea, M. Baran, R. Szymczak, H. Szymczak, M. Mücksch, F. Haider, R. Tidecks, Influence of cation substitution on the magnetic properties of the $FeCr_2S_4$ ferrimagnet. J. Phys. Chem. Sol. 66 (2005) 2040–2043.

36. R. Tong, Z. Yang, C. Shen, X. Zhu, Y. Sun, L. Li, S. Zhang, L. Pi, Z. Qu, Y. Zhang, Disorder-induced orbital glass state in $FeCr_2S_4$, EPL 89, (2010) 57002.

37. C. Shen, Z. Yang, R. Tong, Z. Zi, W. Song, Y. Sun, L. Pi, Y. Zhang, Magnetic anomaly around orbital ordering in $FeCr_2S_4$, J. Appl. Phys. 109 (2011) 07E144.

38. T. Kohout, A. Kosterov, M. Jackson, L.J. Pesonen, G. Kletetschka, M. Lehtinen, Low-temperature magnetic properties of the Neuschwanstein EL6 meteorite, Earth Planet. Sci. Let. 261 (2007) 143–151.

39. T. Kohout, A. Kosterov, J. Haloda, P. Tycova, R. Zboril, Low-temperature magnetic properties of iron-bearing sulfides and their contribution to magnetism of cometary bodies, Icarus 208 (2010) 955–962.

40. J. Cuda, T. Kohout, J. Tucek, J. Haloda, J. Filip, R. Prucek, R. Zboril, Low-temperature magnetic transition in troilite: A simple marker for highly stoichiometric FeS systems, J. Geophys. Res. 116 (2011) B11205.

41. V. Tsurkan, M. Lohmann, H.-A.K. von Nidda, A. Loidl, S. Horn, R. Tidecks, Electron-spin-resonance studies of the ferrimagnetic semiconductor $FeCr_2S_4$, Physical Review B 63 (2001) 125209.

42. Z. Klencsár, E. Kuzmann, Z. Homonnay, A. Vértes, A. Simopoulos, E. Devlin, G. Kallias, Interplay between magnetic order and the vibrational state of Fe in $FeCr_2S_4$, J. Phys. Chem. Solids 64 (2003) 325–331.

43. E. Biasi, C.A. Ramos, R.D. Zysler, Size and anisotropy determination by ferromagnetic resonance in dispersed magnetic nanoparticle systems, J. Magn. Magn. Mater. 262 (2003) 235–241.

44. R.E. Kopp, B.P. Weiss, A.C. Maloof, H. Vali, C.Z. Nash, J.L. Kirschvink, Chains, clumps, and strings: Magnetofossil taphonomy with ferromagnetic resonance spectroscopy, Earth Planet. Sci. Lett. 247 (2006) 10–25.

45. D.L. Griscom, Ferromagnetic resonance condition and powder pattern analysis for dilute, spherical, single-domain particles of cubic crystal structure, J. Mag. Res. 45 (1981) 81–87.

46. J. Nowok, V.I. Stenberg, ESR study of pyrrhotite iron vacancies and the adsorption of CO and $H_2S$, App. Surf. Sci. 29 (1987) 463–473.

47. J. Nowok, V.I. Stenberg, Fe(III) ESR-signal splitting in unoxidized and oxidized semimagnetic pyrrhotite, $Fe_7S_8$, Solid State Commun. 66 (1988) 835–840.

48. W. Kündig, Evaluation of Mössbauer spectra for $^{57}Fe$, Nucl. Instr. Meth. 48 (1967) 219–228.

49. J.A. Morice, L.V.C. Rees, D.T. Rickard, Mössbauer studies of iron sulphides, J. Inorg. Nucl. Chem. 3 (1969) 3797–3802.

50. J.M.D. Coey, M.R. Spender, A.H. Morrish, The magnetic structure of the spinel $Fe_3S_4$, Solid State Comm. 8 (1970) 1605–1608.

51. E. Riedel, R. Karl, Mössbauer Studies of Thiospinels. III. The System $FeCr_2S_4$–$FeIn_2S_4$, J. Solid State Chem. 38 (1981) 40–47.

52. H. Stanjek, E. Murad, Comparison of pedogenic and sedimentary greigite by X-ray diffraction and Mössbauer spectroscopy, Clays Clay Miner. 42 (1994) 451–454.

53. I.S. Lyubutin, S.S. Starchikov, C.-R. Lin, S.-Z. Lu, M.O. Shaikh, K.O. Funtov, T.V. Dmitrieva, S.G. Ovchinnikov, I.S. Edelman, R. Ivantsov, Magnetic, structural, and electronic properties of iron sulfide $Fe_3S_4$ nanoparticles synthesized by the polyol mediated process, J. Nanopart. Res. 15 (2013) 1397.

54. D. Satuła, K. Szymański, L. Dobrzyński, V.H. Tran, R. Troć, Mössbauer data analysis based on invariants and application to $UFe_5Sn$, Phys. Rev. B 78 (2008) 014411.

55. K. Szymański, D. Satuła, L. Dobrzyński, K. Rećko, W. Olszewski, K. Brzózka, J. Jankowska-Kisielińska, The method of invariants in $^{57}Fe$ Mössbauer spectroscopy on selected examples, J. Phys.: Conf. Ser. 217 (2010) 012010.

56. Z. Klencsár, MossWinn manual. http://www.mosswinn.com/downloads/mosswinn.pdf, 2014.

57. W.M. Skinner, H.W. Nesbitt, A.R. Pratt, XPS identification of bulk hole defects and itinerant Fe 3d electrons in natural troilite (FeS), Geochim. Cosmochim. Acta 68 (2004) 2259–2263.